ICAS 2020 SHANGHAI
International Council of the Aeronautical Sciences
32nd Congress of the International Council of the Aeronautical Sciences
September 6-10, 2021
Pudong Shangri-La, Shanghai, China

AERODYNAMIC DESIGN OPTIMIZAITON OF HYPERSONIC WING OVER WIDE MACH-NUMBER RANGE CONSIDERING LIFT MATCHING

Yang Zhang, Zhong-Hua Han*, Fei Liu, Chen-Zhou Xu

Institute of Aerodynamic and Multidisciplinary Design Optimization, National Key Laboratory of Science and Technology on Aerodynamic Design and Research, School of Aeronautics, Northwestern Polytechnical University, Xi'an 710072, P. R. China

Abstract

Aerodynamic shape optimization of a hypersonic aircraft over a wide Mach-number range is still challenging, due to the difficulties in cutting down the huge computational cost of high-fidelity CFD simulations and the reasonable compromise between aerodynamic performances at different speed ranges. To address this problem, by applying surrogate-based optimization algorithm, this paper newly proposes a wide-Mach-number-range optimization method considering lift matching, which could improve the usable lift-to-drag ratio (L/D) of the wing when its lift matches the weight of aircraft at different speed ranges. A RANS (Reynolds averaged Navier-Stokes) flow solver is adopted to evaluate objective and constraint functions; Kriging surrogate model combined with a parallel infill-sampling method and a multi-round strategy are employed to find the global optimum. First, aerodynamic performance of the baseline configuration of a hypersonic wing is evaluated and analyzed, and the results show that the wing has a reasonable maximum L/Ds but insufficient usable L/Ds. Then, to increase usable L/Ds of the wing over a wide Mach-number range, planform shape optimization and profile shape optimization are conducted, and significant improvement has been observed. Results show that the hypersonic and supersonic useable L/D of the optimized wing are increased by 10.08% and 29.21% respectively, under the premise that the take-off lift at low speed does not decrease and a better performance over a wide Mach-number range is obtained, which verify the effectiveness of the proposed method.

Keywords: aerodynamic shape optimization; surrogate-based optimization; hypersonic wing; wide Mach-number range; lift matching

1. Introduction

During the past few years, with the rapid development of hypersonic aircraft design technology, several hypersonic vehicles such as X-43[1] and X-51[2] have carried out flight test successfully, indicating that the fundamental theory for hypersonic flight has already made significant breakthroughs. In the next few decades hypersonic vehicles will develop towards wider speed range and wider aerospace range, and even ultimately achieve single-stage-to-orbit vehicle to supply efficient, reliable and cheap aerospace transportation. One of the greatest concerns for a wide Mach-number range hypersonic transport aircraft design is the reasonable compromise between aerodynamic performances over a wide speed range, as aerodynamic shape requirements are often contradictory to each other[3] when flying at different Mach-number ranges. The traditional design method of “cut-and-try” is hard to be competent[4], and aerodynamic design optimization technology assisted with numerical optimization algorithms is becoming a promising method to compromise performance in various speed ranges.

Over the past 30 years, significant progress has been made in applying numerical optimization algorithms to aerodynamic design optimization of hypersonic vehicles. Since 2008, gradient-based optimization method has been employed by researchers from JAXA in the development of hypersonic transportation in Japan. In 2008, Ueno[5] conducted aerodynamic shape optimization of 2-D profiles for a hypersonic transport considering both hypersonic and transonic performances, and the work

was advanced into a 3-D wing configuration design[6] two years later, where the lower surface of the vehicle was found to be the key design factor to obtain a well-balanced aerodynamic performance covering a wide range of Mach numbers. Then, in 2013, they made an evaluation of low-speed aerodynamic performance of the optimized configuration[7]. In 2019, Han [4] developed a surrogate-based aerodynamic shape optimization method to optimize hypersonic flows considering transonic performance, and conducted wide Mach-number-range shape optimization of airfoil and wing successfully.

A lot of research work have proved the feasibility and potential of using aerodynamic design optimization technology to improve wide Mach-number range performance of a hypersonic aircraft, and the motivation of this paper is to use efficient global optimization based on surrogate model (surrogate-based optimization, SBO)[8]-[10] to address a wide Mach-number range aerodynamic design problem that useable L/D of a configuration can be severely insufficient when aerodynamic lift matches its weight at some speed ranges. First, aerodynamic performance of the baseline wing over a wide speed range is evaluated to make sense the concept of lift matching. Then a multi-round surrogate-based optimization considering lift matching constraint is conducted based on the baseline configuration. In detail, the design optimization is carried out in three steps. For the first step, the planform of baseline wing is optimized to maximize the usable L/Ds at Mach number both 6.0 and 2.0 subject to the take-off lift constraint at Mach number 0.3. For the second step, profile optimization of the wing with respect to 54 design variables are performed. For the last step, planform and profile integrated optimization is conducted with respect to 61 design variables. Finally, the aerodynamic performance of the baseline and optimized wings are evaluated and compared over a wide range of Mach-number.

This paper continues in Section 2 with the validation of RANS flow solver used for optimization. In Section 3, the optimization framework based on surrogate model is introduced, and the aerodynamic performance over a wide Mach-number range of the baseline wing configuration are evaluated in section 4 In section 5, planform shape optimization, profile shape optimization and planform/profile integrated optimization are carried out in turn to improve aerodynamic performance of baseline wing over wide speed range. The last section is for some conclusions and outlooks.

2. Flow Slover

An accurate, efficient, and robust CFD solver plays an important role in the process chain of an aircraft aerodynamic shape optimization. A RANS flow solver is validated for aerodynamic shape optimization. Please note that for simplicity, real gas effect is not taken into account in the simulation of hypersonic flows in this article, due to the fact that the influence is slight under low hypersonic condition (Ma<7).

2.1 Validation of RANS flow solver for transonic flows

To validate the RANS flow solver, it is firstly used to simulate the transonic flow ($Ma = 0.75, \mathrm{Re} = 3.0\times10^6, C_L = 0.500 \pm 0.001$) over a DLR F6 configuration. A Roe scheme is used for spatial discretization and a k-ω SST turbulence model is used for turbulent closure. The surface structured grid is sketched in Figure 1 and the comparison of computed pressure distribution and experimental data[11] is shown in Figure 2, where η represents the unified position along the wing span.

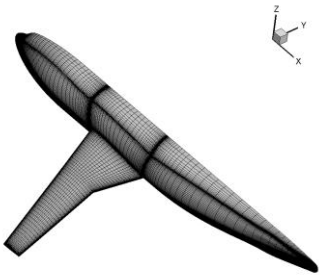

Figure 1 Sketch of surface grid for transonic F6 configuration

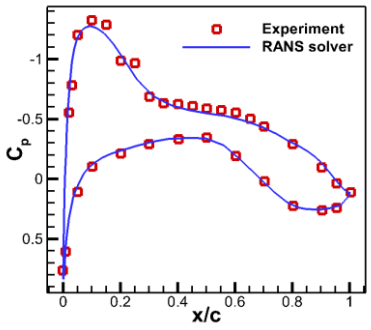

(a) η =0.239

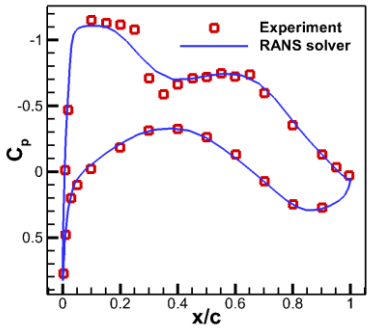

(b) η =0.411

Figure 2 Comparison of computed pressure distribution and experimental data at transonic condition ($Ma = 0.75, \mathrm{Re} = 3.0\times10^6, C_L = 0.500 \pm 0.001$)

2.2 Validation of RANS flow solver for hypersonic flows

The hypersonic flow over a square-section-shape missile is simulated. The computation is performed at Ma=4.5, $\mathrm{Re} = 1.312\times10^7$, γ=0°, where γ represents the roll angle. An AUSM (Advection Upstream Splitting Method) scheme is used for spatial discretization and a k-ω SST turbulence model is used for turbulent closure. A structured grid is used and the number of gird points is 2.5 million (Figure 3 shows the surface grid). The comparison of computed force coefficient and experimental data[12] is shown in Figure 4. It can be seen that the computed lift and moment coefficients are in good agreement with the experimental data at different angles of attack, while drag coefficient shows little discrepancy with the experiment, due to the fact that flow transition is not considered in our simulation.

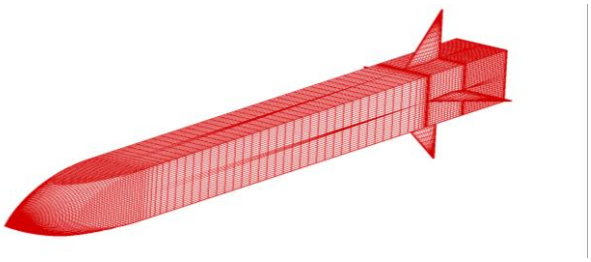

Figure 3 Surface grid for a square-section-shape missile

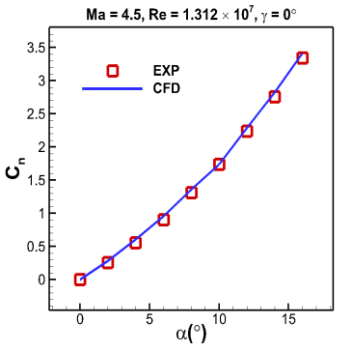

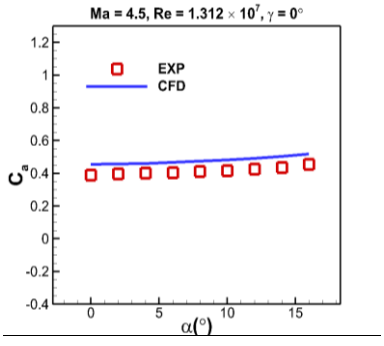

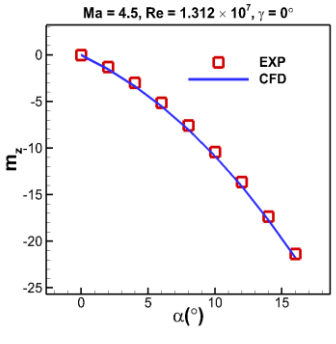

Figure 4 Comparison of computed force coefficients and experimental data for a square section shape missile (Ma=4.5, $\mathrm{Re} = 1.312\times10^7$, γ=0°)

3. Surrogate-Based Optimization Framework

In this paper, an in-house code based on efficient global surrogate-based optimization method called "SurroOpt"[13] is employed to carry out aerodynamic shape optimization of a hypersonic wing. It can be used to solve arbitrary single and multi-objective, unconstrained and constrained optimization

problems with continuous and smooth design space. It has built-in modern design of experiments (DoE) methods for deterministic computer experiments, such as Latin hypercube sampling, uniform design, quasi Monte Carlo design, etc. A variety of surrogate models, such as polynomial response surface model, kriging and its variants (gradient-enhanced kriging, cokriging, and hierarchical kriging), radial-based functions, artificial neural network, support-vector regression, have been implemented. A couple of infill-sampling criteria and dedicated constraint handling methods are available, such as minimizing surrogate prediction (MSP), maximizing expected improvement (EI), maximizing probability of improvement, maximizing mean-squared error (MSE), minimizing lower-confidence bounding (LCB), target searching, and combined parallel infill-sampling criteria. Some well-accepted and matured optimization algorithms, such as Hooke&Jeeves pattern search, simplex, quasi-Newton's method, sequential quadratic programming, single/multi objective genetic algorithms, are employed to solve the sub-optimization(s), in which the cost function(s) and constraint function(s) are evaluated by the cheap-to-evaluate surrogate models and the computational cost is negligible compared to a CFD simulation. SurroOpt has been paralleled by the technique of MPI (message passing interface), which allows the user to run the code with multiple cores to speed up the optimization process.

In this paper, SurroOpt is used to solve the following constrained single-objective optimization problem

$$\begin{aligned} &min. \quad f_{obj}\left(\boldsymbol{x}\right) \\ &w.r.t. \quad \boldsymbol{x}_l \le \boldsymbol{x} \le \boldsymbol{x}_u \\ &s.t. \quad h_i\left(\boldsymbol{x}\right)=0,\ i=1,\cdots,N_E \\ &\qquad g_j\left(\boldsymbol{x}\right)\ge 0,\ j=1,\cdots,N_C \end{aligned} \tag{1}$$

where f_{obj} is the objective function; $\boldsymbol{x}_l$ and $\boldsymbol{x}_u$ are the lower and upper bounds of the design variables $\boldsymbol{x}\in\mathbb{R}^m$, respectively; $h_i\left(\boldsymbol{x}\right)$ and $g_j\left(\boldsymbol{x}\right)$ denote *i*-th equality constraint function and *j*-th inequality constraint function, respectively, while N_E and N_C are the numbers of equality and inequality constraints, respectively. The optimization framework of SurroOpt is sketched in Figure 5. After the optimization model is defined, the following steps will be taken to obtain an optimized configuration.

1) First, initial sample points are chosen by a DoE method. The sample points are generated by parameterization method. The grid for every sample configuration is generated automatically. The functional responses are then evaluated in parallel by CFD code.

2) Second, initial kriging models for the objective and constraint functions are tuned and built, based on the sampled dataset. The optimized model parameters are then stored and used to efficiently predict the values of the objective and constraint functions at any untried point in the design space.

3) Third, the parallel infill-sampling criteria, combing the MSP, EI, MSE, LCB, PI are used and sub-optimizations are executed based on the cheap-to-evaluated kriging models, using a hybrid method combing GA, Hooke&Jeeves local searching and gradient-based optimization, which in turn simultaneously generates five sample points to be evaluated in parallel by the CFD code again.

4) Fourth, the newly selected sample points as well as the functional responses are augmented to the sampled database and the kriging models are updated.

Note that steps 3 and 4 are repeated until one of the termination conditions is satisfied.

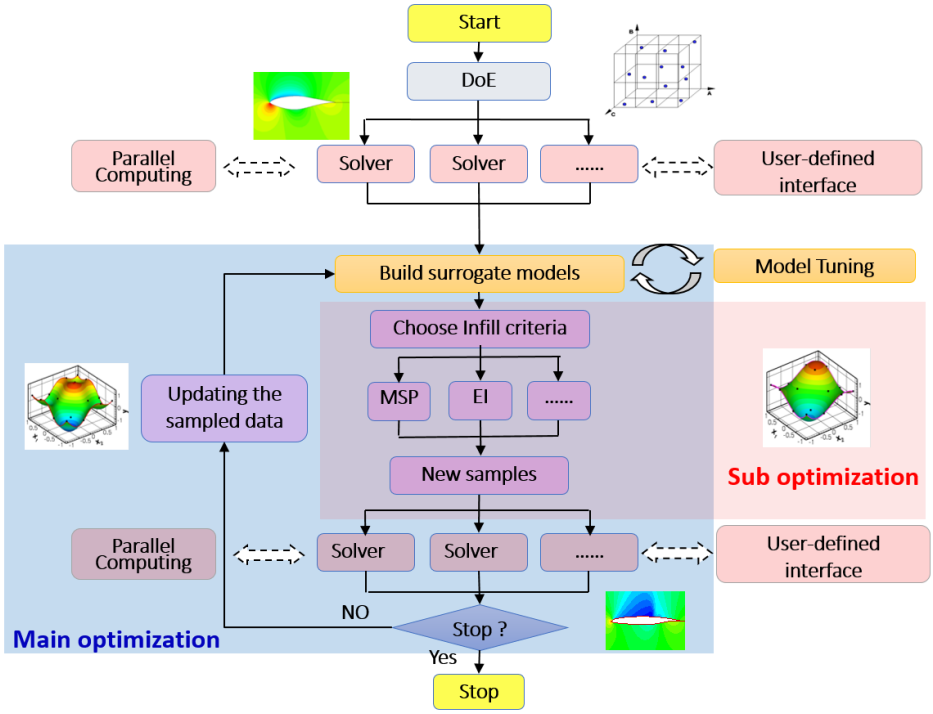

Figure 5 Framework of an in-house surrogate-based optimizer: SurroOpt

4. Aerodynamic Performance of Baseline Wing over a Wide Mach-Number Range

The planar shape of baseline wing is referred to “Sanger” hypersonic transport vehicle[15][16] (Figure 6), and the wide Mach-number range airfoil NPU-Hyper-04[17](Figure 7) is mounted along flow direction at root, kink and tip of the wing. Detailed parameters of baseline wing are listed in Table 1.

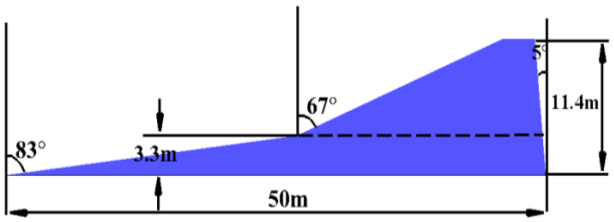

Figure 6 Planar shape of the wing

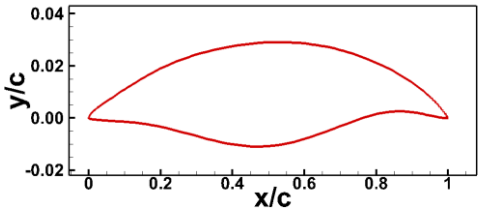

Figure 7 NPU-Hyper-04 airfoil

Table 1 Parameters of the plane shape

shape parameters	value
inner root chord	50m
inner wing leading edge sweep angle	83°
inner wing trailing edge sweep angle	5°
inner wing span	3.3m
outer wing leading edge sweep angle	67°
outer wing trailing edge sweep angle	5°
outer wing span	8.1m

Aerodynamic performance of the baseline wing is evaluated under three flow conditions: (a) Subsonic state: the Mach-number is set to 0.3 and the altitude is 0 km. This is a typical take-off state, and the attack alpha is fixed at 10 degree. (b) Supersonic design state: the Mach-number is set to 2.0 and the altitude is 10km. (c) Hypersonic design state: the Mach-number is set to 6.0 and the altitude is

25km.

Figure 8 shows curve of lift-to-drag ratio (L/D) of the baseline wing at supersonic and hypersonic states. It can be seen that maximum supersonic L/D of the wing is obtained at attack angle of 4 degree, and the maximum hypersonic L/D is obtained at attack angle of 4.5 degree. Dimensional force of the wing at take-off state and maximum L/D states under supersonic and hypersonic flow conditions is listed in Table 2, from which we can find that lift of the wing at supersonic maximum L/D state is 3.0 times larger than the take-off lift, and the lift at hypersonic maximum L/D state is 1.1 times larger than the take-off lift. However, when a wide Mach-number range hypersonic vehicle takes off from subsonic state and experiences accelerating, climbing, up to hypersonic cruise, its weight balanced by aerodynamic lift will decrease with fuel consumption, which reveals that lift needed by aircraft also decreases gradually as time goes on. Therefore, the significant difference between take-off lift and lift at maximum L/D state in both supersonic and hypersonic conditions indicates that the baseline wing could not keeping flying at maximum L/D state in neither supersonic nor hypersonic conditions.

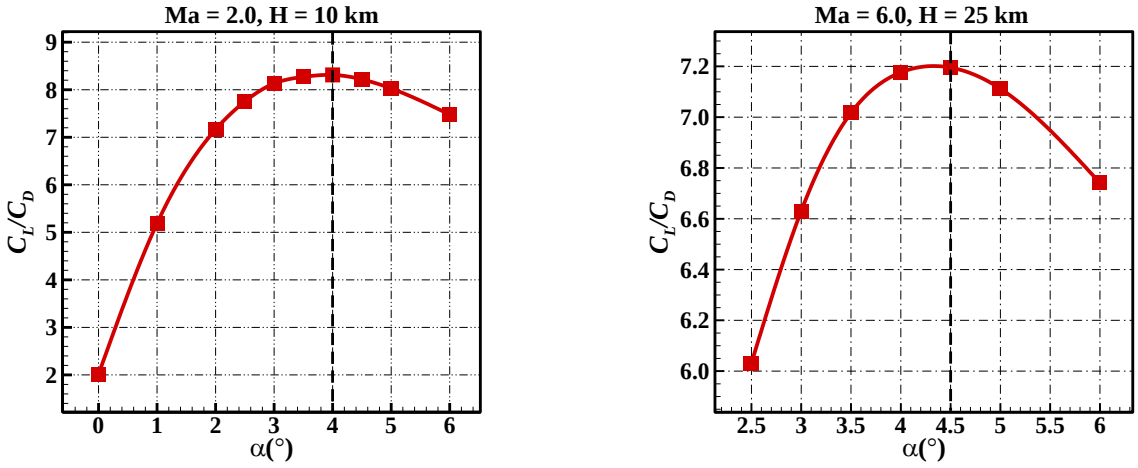

(a) Supersonic: *Ma=2.0, H=10km* (b) Hypersonic:*Ma=6.0, H=25km*

Figure 8 L/Ds of Sanger wing at supersonic and hypersonic states

Table 2 Aerodynamic characteristics in different flight states

	Lift(ton)	L/D
Typical take-off state $(Ma=0.3, H=0km, \alpha=10°)$	64.28	5.98
Maximum *L/D* state in supersonic condition $(Ma=2.0, H=10km, \alpha=4°)$	192.21	8.31
Maximum *L/D* state in hypersonic condition $(Ma=6.0, H=25km, \alpha=4.5°)$	70.31	7.20

Assume that the weight of a hypersonic aircraft at supersonic design state reduce to 0.85 times than the weight at the take-off state, and further reduce to 0.7 times than the take-off weight when it accelerates to hypersonic design state to conform with the trend that weight of wide Mach-number range aircraft reduces gradually in real flight. Then lift of baseline wing at typical take-off state is assumed to be equal to the take-off weight, and Table 3 shows the real-time weight at different design states according to assumptions above and usable L/Ds of baseline wing when aerodynamic lift balances weight at different Mach numbers. Results in Table 3 reveal that usable L/Ds in supersonic and hypersonic conditions when lift matches weight are much less than maximum L/Ds at corresponding states, which is especially severe in supersonic condition and the usable L/D reduces 46.45% compared to maximum L/D. Above analysis indicates that maximum L/D of baseline wing in

different speed range is barely satisfactory, but usable L/D when lift equals its weight is quite insufficient (especially in the case of supersonic speed), and the wide Mach-number range aerodynamic performance needs to be improved.

Table 3 Aerodynamic characteristics in various flight states

	Weight(ton)	L/D when lift balances weight
Typical take-off state $(Ma=0.3, H=0km, \alpha=10°)$	64.28	5.98
Supersonic design state $(Ma=0.3, H=0km, \alpha=10°)$	54.64	4.45
Hypersonic design state $(Ma=0.3, H=0km, \alpha=10°)$	45.00	6.65

In this paper, aerodynamic shape optimization of wide Mach-number range wing considering lift matching is proposed to address this problem. The constraint of lift matching means that in the design optimization of a hypersonic wing over a wide Mach-number range, it is necessary to ensure that the optimization objective is L/D when the lift equals to the corresponding weight at different speed ranges so that the optimal L/D can be usable in practical flight.

5. Wide Mach-Number Range Shape Optimization of Baseline Wing

In this section, aerodynamic design optimization is conducted to improve its usable L/Ds when the aerodynamic lift and weight are matched over a wide Mach-number range. Planform shape optimization, profile shape optimization and planform/profile integrated optimization are conducted in turn.

5.1 Shape optimization of wing planform

A two-round design optimization of planar shape of the baseline wing configuration is firstly carried out.

a) Optimization problem set up

The design states are listed in Table 4. It is observed that fixed lift is applied in both supersonic and hypersonic conditions, while fixed angle is used in subsonic condition, which is determined by the demand of considering lift matching. A mixed grid is employed and the number of grid points is 1.0 to 1.5 million, which varies with different wing configurations (see Figure 9).

Table 4 Design points at various flight states

	Mach-number	Altitude(km)	Fixed $(°)$ angle or lift (ton)
Typical take-off state	0.3	0	fixed angle: $10°$
Supersonic design state	2.0	10	fixed lift: 54.64
Hypersonic design state	6.0	25	fixed lift: 45.00

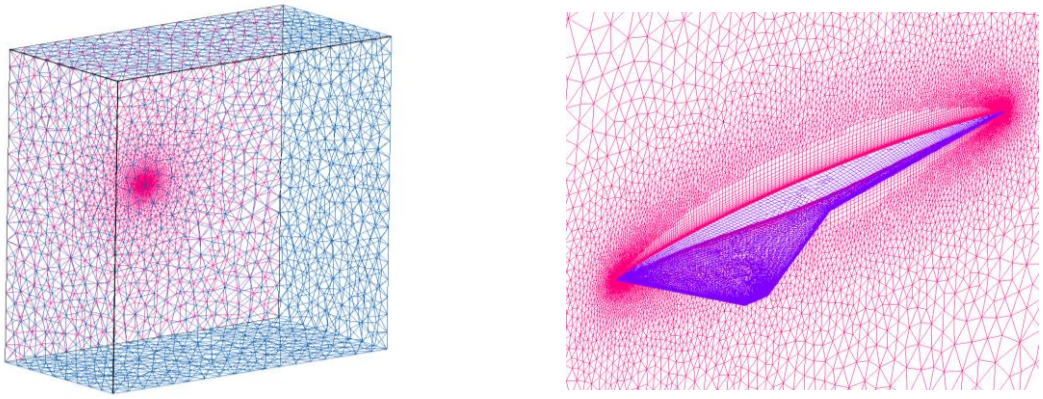

Figure 9 Schematics of computational grid

The objective is to minimize drag at both supersonic and hypersonic design states, with lift at typical take-off state of wing constrained. The optimization mathematical model is of the form:

$$\begin{aligned} max \quad & f_{obj}\left(\boldsymbol{x}\right) = A_1 * D_{Ma=2.0} / D_{0,Ma=2.0} + A_2 * D_{Ma=6.0} / D_{0,Ma=6.0} \\ s.t. \quad & L_{Ma=0.3} \geq W_{Ma=0.3} \\ & L_{Ma=2.0} = W_{Ma=2.0} \\ & L_{Ma=6.0} = W_{Ma=6.0} \end{aligned} \tag{2}$$

where $D_{Ma=2.0}$ and $D_{Ma=6.0}$ represent drag force of wing at supersonic and hypersonic design state, respectively; $L_{Ma=0.3}$, $L_{Ma=2.0}$ and $L_{Ma=6.0}$ represent the lift at three design points; $W_{Ma=0.3}$, $W_{Ma=2.0}$ and $W_{Ma=6.0}$ represent weight at take-off state, supersonic design state and hypersonic state respectively, and value of these weight is the same as that in Table 3; All the notations with subscript "0" mean baseline; A_1 and A_2 are the weight coefficients of objectives, which are chosen according to design experience. In this article we use $A_1 = A_2 = 0.5$.

The objective and constraints are defined by dimensional force rather than commonly used dimensionless force coefficient, and there exist two equality constraints to guarantee aerodynamic lift equals real-time weight at supersonic and hypersonic states which are difficult to cope with by optimization algorithm, and in optimization the two constraints are realized by conducting CFD calculation at fixed lift force.

The design variables of planform optimization consist of wing area, inner wing leading edge sweep angle, outer wing leading edge sweep angle, inner wing trailing edge sweep angle, outer wing trailing edge sweep angle, kink chord and wingtip chord. The design space of these seven planform design variables is listed in Table 5. In the optimization, 20 initial sample points are generated by LHS and Kriging surrogate model with EI+MSP+LCB+PI+MSE parallel infilling sample criterion is used.

Table 5 The design space of wing's planar shape

shape parameters	design space
wing area	（180m^2，270m^2）
inner wing leading edge sweep angle	（60°，85°）
outer wing leading edge sweep angle	（35°，75°）
inner wing trailing edge sweep angle	（-30°，45°）
outer wing trailing edge sweep angle	（-25°，30°）
kink chord	（0.25．0.60）
wingtip chord	（0.03．0.20）

b) Optimization result

Figure 10 shows the convergence history of objective function after two rounds of optimization. Due to the fact that the optimized wing had changed a lot in shape compared with the baseline, the design space did not include the optimum and some design variables soon reach the boundary of design space in the first-round optimization. Thus, based on the optimized profile in the first-round, the design space of these design variables is redefined, and a second-round optimization is performed. The two-round design optimization stopped after 800 high-fidelity simulations. The optimal configuration obtained is marked as Opt-1.

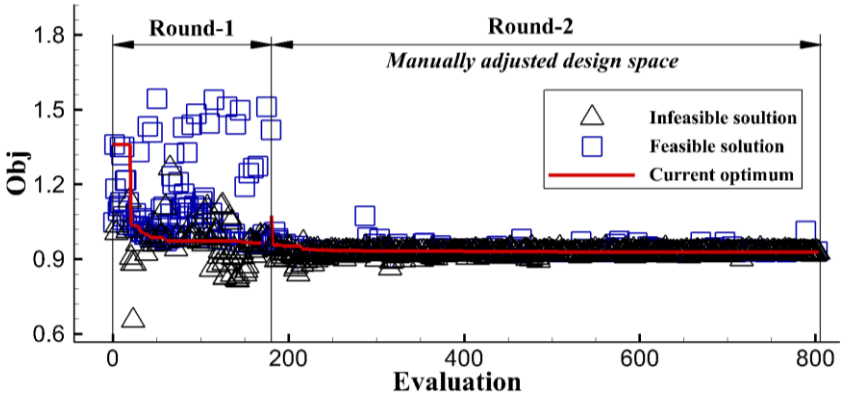

Figure 10 Convergence history and infill sampling in a two-round optimization of wing planform

Fig. 11 shows a comparison of planar shapes of baseline and optimized wing, and the comparison of the detailed parameters are listed in Figure 11. It can be seen that area, chord length and average geometric chord length of the optimized wing are significantly reduced, but the span length increases a bit, which makes the optimized wing has obviously larger aspect ratio than baseline. The leading-edge sweep angle of both inner and outer optimized wing has also become smaller, and the trailing edge angles change from forward sweep to backward sweep.

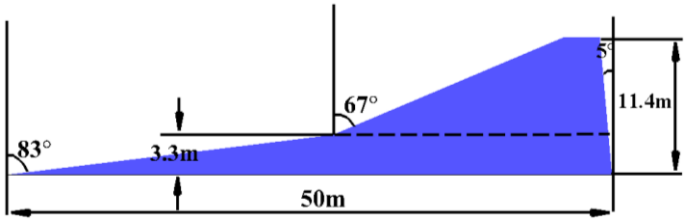

(a) Planar shape of baseline wing

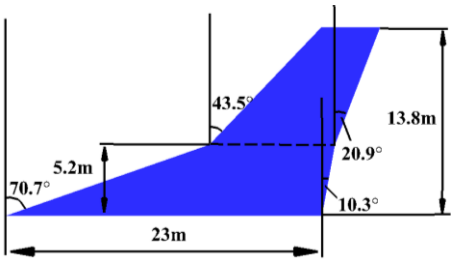

(b) Planar shape of optimized wing

Figure 11 Comparison of planar shape between the optimized wing and baseline

Table 6 Comparison of planar shape parameters between baseline and Opt-1

shape parameters	Baseline	Optimized wing
wing area	224.56m^2	140.93m^2
inner wing leading edge sweep angle	83°	70.65°

outer wing leading edge sweep angle	67°	43.47°
inner wing trailing edge sweep angle	5°	-10.31°
outer wing trailing edge sweep angle	5°	-20.93°
kink chord	0.4550	0.3972
wingtip chord	0.0600	0.1856

Figure 12 is a comparison of aerodynamic characteristics curve of baseline and the optimized wing at supersonic state. From the comparison of dimensionless force coefficient, both lift coefficient and drag coefficient of the optimized wing are larger than that of baseline at the same attack angle. But it presents a totally opposite trend if curves of dimensional force are analyzed, and the lift as well as drag force of the optimized wing is smaller than that of baseline at the same attack angle. Actually, as area of the wing is constantly changing during the optimization, comparison of dimensionless force coefficients can be misleading and dimensional force should be directly compared. From the comparison of lift force and drag force curve, it can be found that both lift and drag force characteristics of the optimized wing varies a lot compared to baseline. Figure 13 is a comparison of aerodynamic characteristics curve of baseline and the optimized wing at hypersonic state, which presents a similar trend as that in supersonic condition.

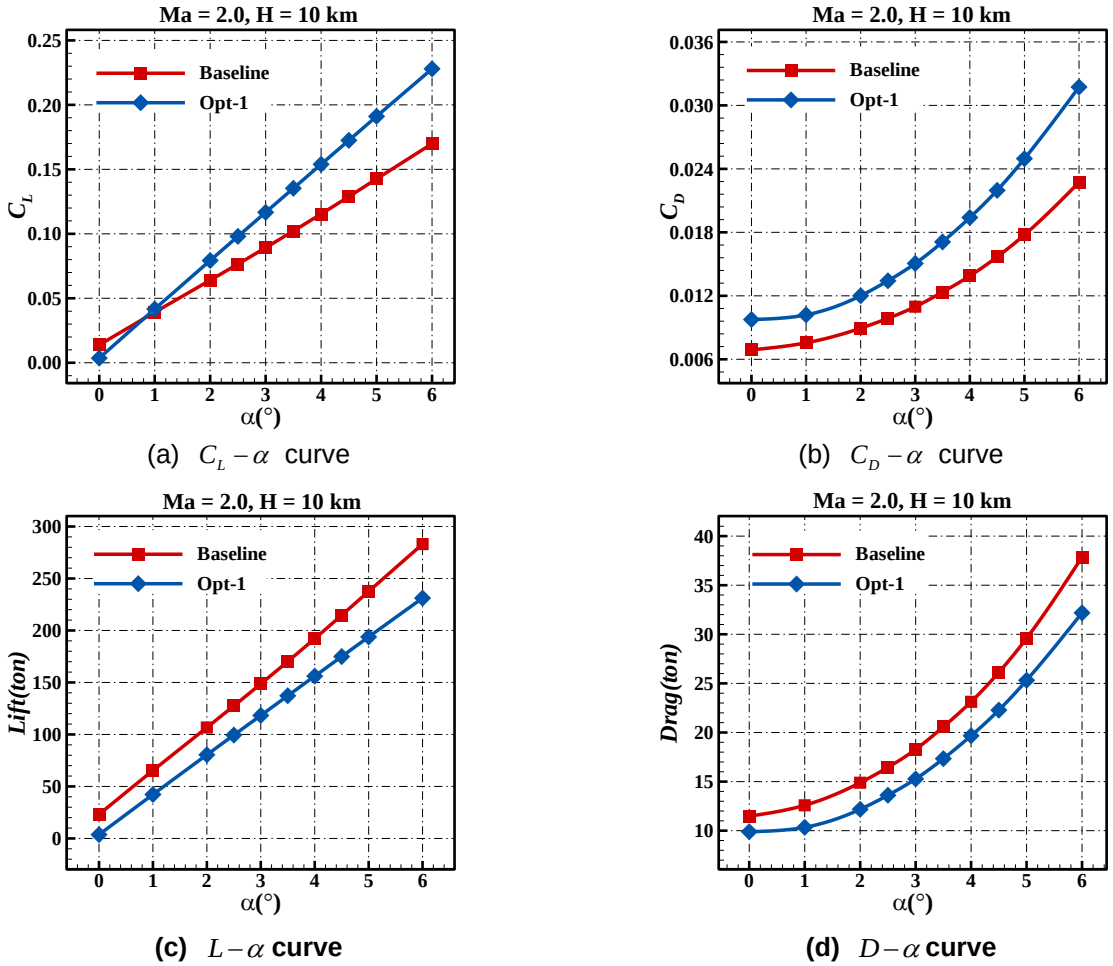

(a) $C_L - \alpha$ curve

(b) $C_D - \alpha$ curve

(c) $L - \alpha$ **curve**

(d) $D - \alpha$ **curve**

Figure 12 Comparison of Aerodynamic characteristic curve at supersonic state $(Ma = 2.0, H = 10km)$

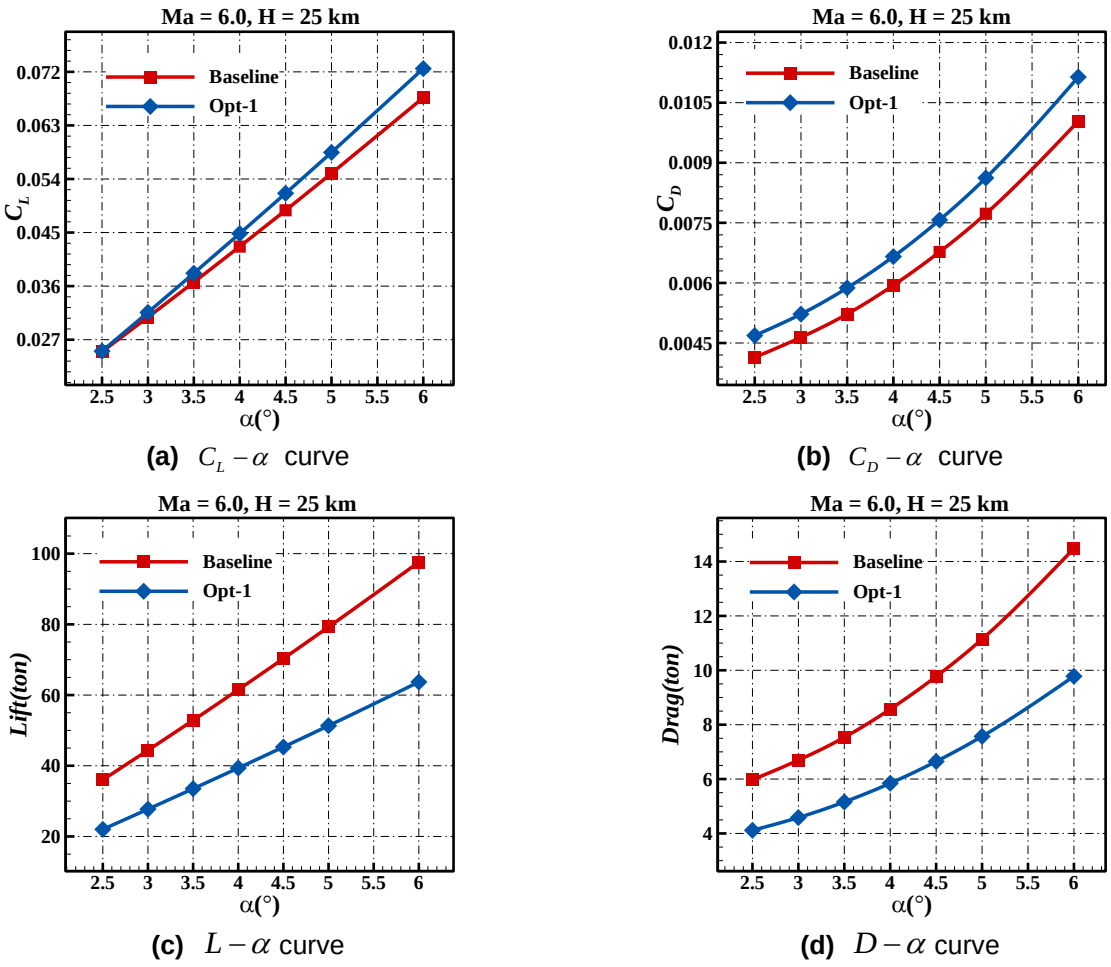

(a) $C_L - \alpha$ curve **(b)** $C_D - \alpha$ curve

(c) $L - \alpha$ curve **(d)** $D - \alpha$ curve

Figure 13 Comparison of Aerodynamic characteristic curve at hypersonic state $(Ma = 6.0, H = 25km)$

Figure 14 and Figure 15 are comparison of $(C_L / C_D) - L$ curves of baseline and Opt-1 at supersonic and hypersonic states. The vertical dashed lines in the two figures indicate values of corresponding weight in supersonic and hypersonic design point respectively, and the intersection point of $(C_L / C_D) - L$ curve and the dashed line represents usable L/D when aerodynamic lift equals the corresponding weight at different Mach-number. It can be seen that though the maximum L/Ds of the optimized wing are reduced both at supersonic and hypersonic states, the optimized wing's usable L/Ds of when lift balances weight are larger than that of baseline, indicating that optimization of L/D over wide Mach-number range considering lift matching achieves some results. Table 7 shows the detailed data of dimensional force and corresponding L/Ds in three design states. The supersonic usable L/D when aerodynamic lift matches the weight is improved to 5.02, which is 12.81% larger than that of baseline wing. The hypersonic usable L/D is increased to 6.81 and is 2.41% than that of baseline wing. Results show that the optimized wing has better aerodynamic performance at both supersonic and hypersonic speed regime. And L/D at typical take-off state has also increased by 5.69% also it is not set as an optimization objective.

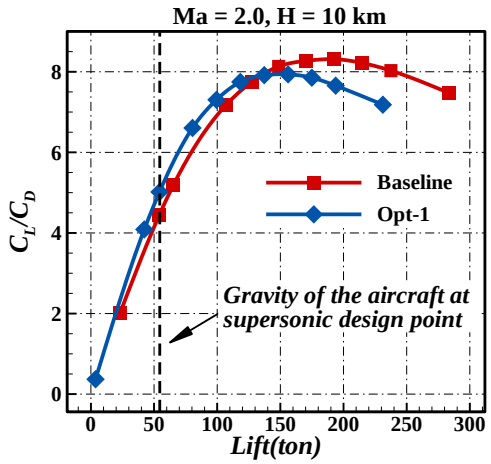

Figure 14 Comparison of $(C_L / C_D) - L$ curve at supersonic typical state $(Ma = 2.0, H = 10km)$

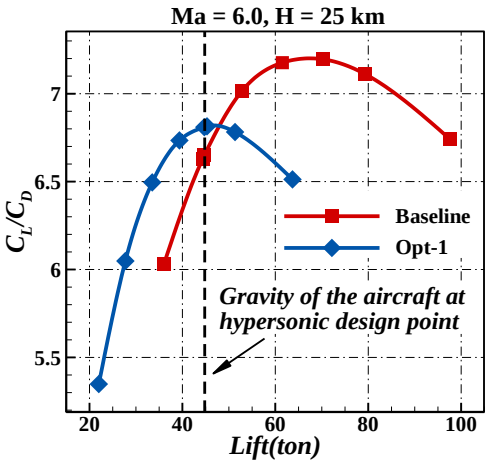

Figure 15 Comparison of $(C_L / C_D) - L$ curve at supersonic typical state $(Ma = 6.0, H = 25km)$

Table 7 Comparison of dimensional force and *L/D* between optimized wing and baseline

		Baseline	Optimum	Improvement
Typical take-off state $(Ma = 0.3, H = 0km, \alpha = 10°)$	*Lift (ton)*	64.28	64.16	/
	Drag (ton)	10.75	10.15	/
	L/D	5.98	6.32	+5.69%
Supersonic design state $(Ma = 2.0, H = 10km)$	*Lift (ton)*	54.28	54.30	/
	Drag (ton)	12.19	10.82	/
	L/D	4.45	5.02	+12.81%
Hypersonic design state $(Ma = 6.0, H = 25km)$	*Lift (ton)*	44.72	44.72	/
	Drag (ton)	6.73	6.55	/
	L/D	6.65	6.81	+2.41%

From the aerodynamic analysis in section 2, when the baseline wing reaches maximum L/D at supersonic and hypersonic design states, its corresponding lift exceeds weight of the aircraft so that the wing cannot fly with maximum L/D, which is particularly severe in supersonic condition. If we merely consider aerodynamic performance at supersonic and hypersonic conditions, usable L/Ds when lift matches weight at these states can be increased by only reducing area of wing, and that is why area of the optimized wing Opt-1 is significantly reduced. However, takeoff lift cannot be sustained if we only reduce wing area without other shape change. And the optimization algorithm comes up with a solution by simultaneously reducing sweep angle of wing and increasing its aspect ratio while reducing area of wing. Figure 16 is the comparison of pressure coefficient contour at typical take-off state $(Ma = 0.3, H = 0km, \alpha = 10°)$, from which we can find that the smaller leading-edge angle of Opt-1 can produce more vortex lift so that the take-off lift can be stained though the wing area is obviously reduced.

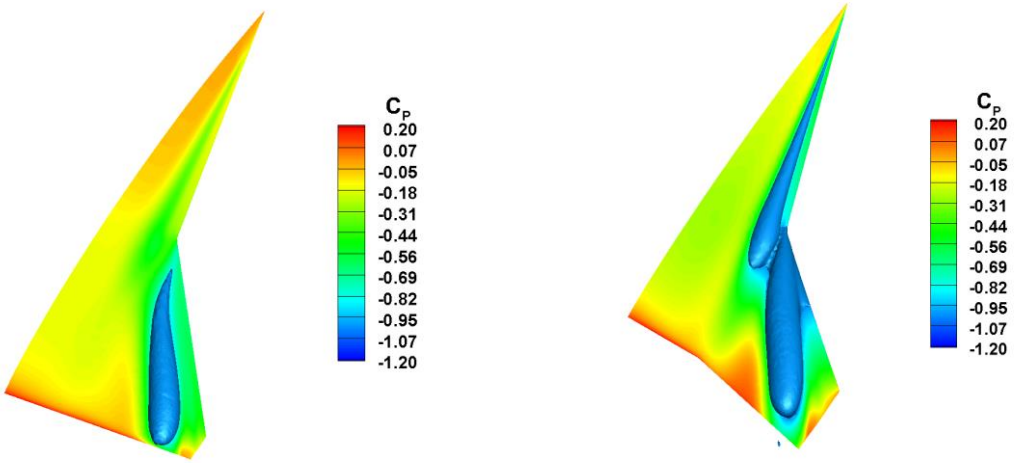

(a) Baseline **(b) Optimized wing**

Figure 16 Comparison of pressure coefficient contours and iso surface (Cp = -1) of baseline (left) and optimal (right) wings at typical take-off state $\left(Ma=0.3, H=0km, \alpha=10°\right)$

5.2 Shape optimization of wing profile

In this section, based on the result obtained by planar shape optimization, profiles at root, kink and tip of the wing are optimized to further improve its wide Mach-number-range aerodynamic performance.

a) Optimization problem set up

The objective is to minimize drag both at supersonic and hypersonic design point, with lift at typical take-off design point of wing being constrained. The optimization mathematical model is of the form:

$$\begin{aligned} max \quad & f_{obj}\left(\boldsymbol{x}\right)=A_1*D_{Ma=2.0}/D_{0,Ma=2.0}+A_2*D_{Ma=6.0}/D_{0,Ma=6.0} \\ s.t. \quad & L_{Ma=0.3}\geq W_{Ma=0.3} \\ & L_{Ma=2.0}=W_{Ma=2.0} \\ & L_{Ma=6.0}=W_{Ma=6.0} \\ & t_{root}\geq t_{0,root}\ ,\ t_{kink}\geq t_{0,kink}\ ,\ t_{tip}\geq t_{0,tip} \\ & R_{root}\geq R_{0,root}\ ,\ R_{kink}\geq R_{0,kink}\ ,\ R_{tip}\geq R_{0,tip} \end{aligned} \tag{3}$$

where t_{root}, t_{kink} and t_{tip} represent relative thickness of profile at root, kink and tip of the wing, R_{root}, R_{kink}, R_{tip} represent leading edge radius of the profile at root, kink and tip of the wing. All the notations with subscript “0” mean baseline.

b) Optimization result

The convergence history of the objective function is plotted in Figure 17. Figure 17 depicts the best observed objective function versus number of CFD simulations; The optimization is terminated after 160 CFD evaluations, and the optimal wing newly obtained is marked as Opt-2.

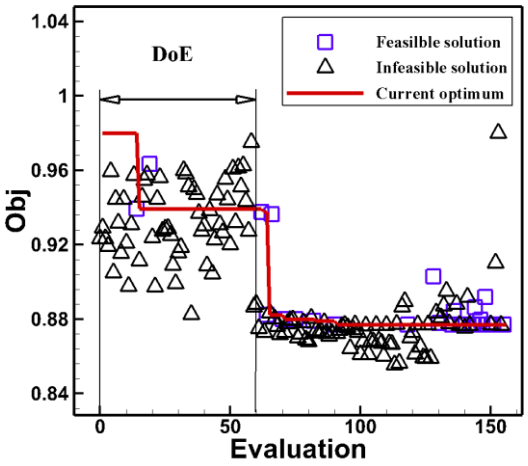

Figure 17 Convergence history and infill sampling in optimization of profile shape

Figure 18 shows a comparison of geometric shapes of baseline airfoils (NPU-Hyper-04) and optimized airfoils at root, kink, and tip. It can be found that airfoils at root, kink and tip of the optimized wing (Opt-2) have similar changing trend. Compared to the baseline airfoil NPU-Hyper-04, the leading edge of upper surface of the optimized airfoils have concave deformations, and the local curvature at trailing edge of lower surface of optimized wings has become smaller, which will help to reduce drag force at supersonic and hypersonic states.

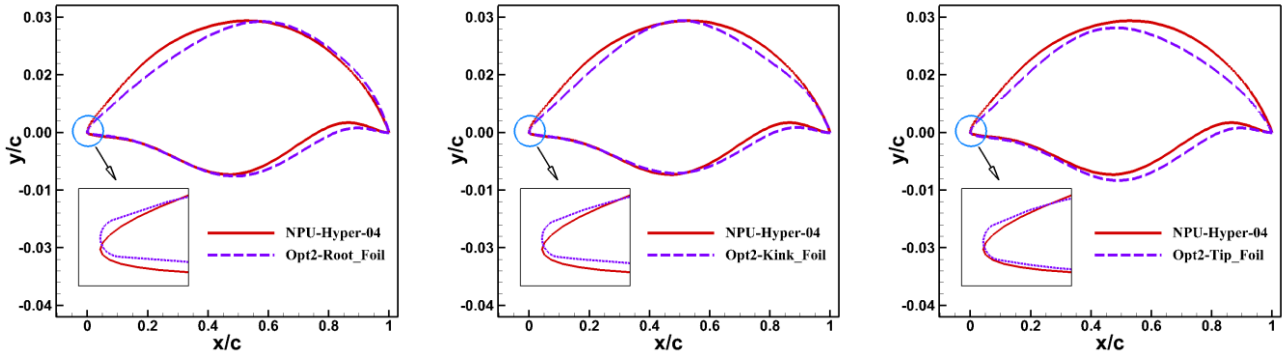

a) Root b) Kink c) Tip

Figure 18 - Comparison of geometric profile at root, kink and tip of double-delta wing

Figure 19 and Figure 20 depict comparison of aerodynamic characteristics curve of baseline and the optimized wings at supersonic and hypersonic states respectively. Unlike the results of planform optimization, compared to Opt-1, we can find that only the drag force characteristic of Opt-2 changes obviously after profile optimization both at supersonic and hypersonic states.

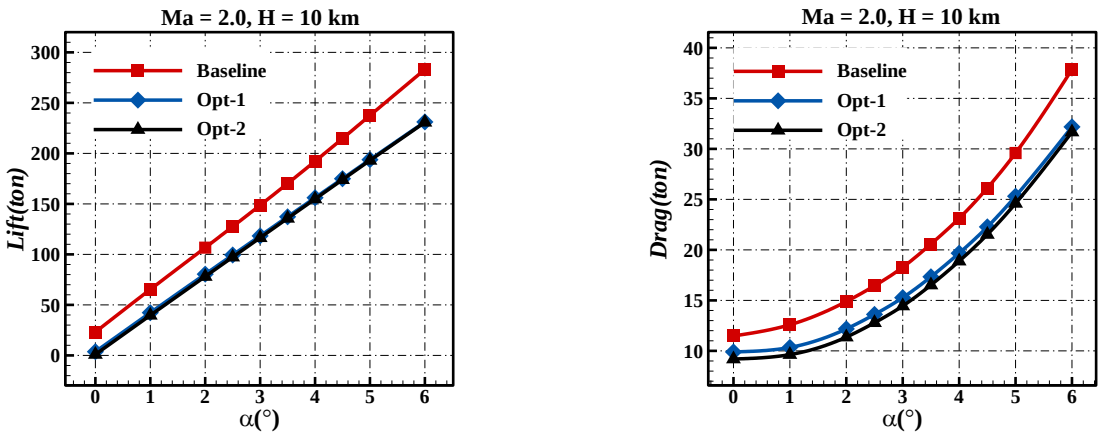

a) $L-\alpha$ curve b) $D-\alpha$ curve

Figure 19 Comparison of Aerodynamic characteristic curve at supersonic state $(Ma=2.0, H=10km)$

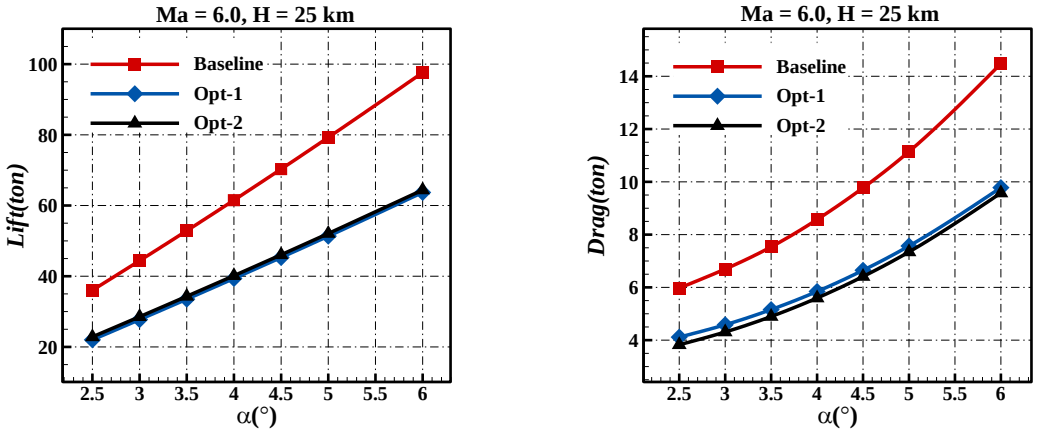

(a) $L-\alpha$ curve **(b)** $D-\alpha$ curve

Figure 20 Comparison of Aerodynamic characteristic curve at supersonic state $(Ma=6.0, H=25km)$

Figure 21 and Figure 22 are comparison of $(C_L/C_D)-L$ curves in supersonic and hypersonic conditions. The vertical dashed lines in the two figures indicate values of corresponding weight in supersonic and hypersonic flight respectively. From intersection point of $(C_L/C_D)-L$ curves and the dashed lines, it can be seen the usable L/Ds of Opt-2 when lift balances weight have been further increased both at supersonic and hypersonic states. The detailed data of dimensional force and corresponding L/Ds in three design states is shown in Table 8. The supersonic usable L/D of optimum-2 when aerodynamic lift balances the weight is further increased to 5.32, which is 19.55% more than that of baseline wing. And the hypersonic usable L/D is further improved to 7.24, which is 8.12% than that of baseline wing. Furthermore, it should be noted that changing trend of $(C_L/C_D)-L$ curve of optimized wing is very different between the result of planform optimization and profile optimization. The $(C_L/C_D)-L$ curve of Opt-1 after planform optimization has an obvious movement in the horizontal direction compared to baseline, but $(C_L/C_D)-L$ curve of Opt-2 after profile optimization only has an obvious movement in the vertical direction compared to baseline. The phenomenon above indicates that planform optimization helps to improve the performance by finding a better matching point of lift, but profile optimization helps to improve the performance mainly by reducing drag.

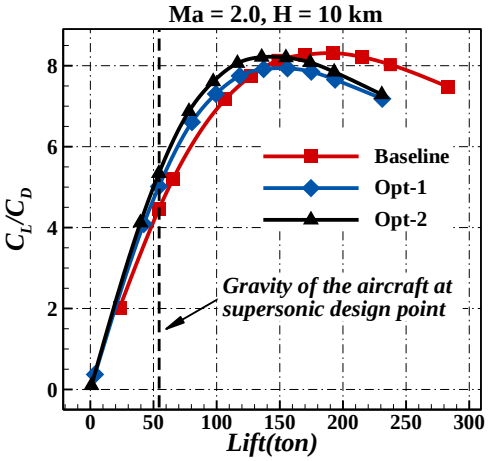

Figure 21 Comparison of $(C_L/C_D)-L$ curve at supersonic typical state $(Ma=2.0, H=10km)$

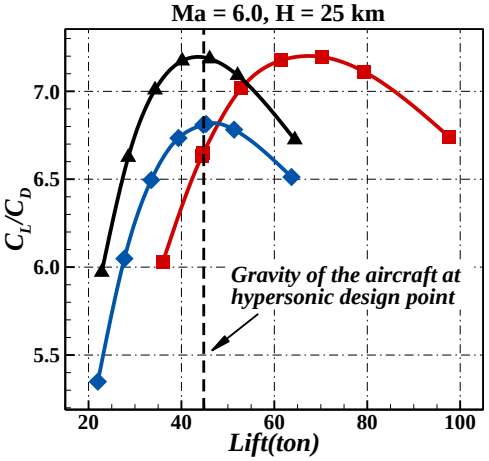

Figure 22 Comparison of $(C_L/C_D)-L$ curve at supersonic typical state $(Ma=6.0, H=25km)$

Table 8 Comparison of dimensional force and *L/D* between optimized wings and baseline

	Typical take-off state	Supersonic design point	Hypersonic design point

	$(Ma=0.3, H=0km, \alpha=10°)$			$(Ma=2.0, H=10km)$			$(Ma=6.0, H=25km)$		
	Lift (ton)	*Drag (ton)*	*L/D*	*Lift (ton)*	*Drag (ton)*	*L/D*	*Lift (ton)*	*Drag (ton)*	*L/D*
Baseline	64.28	10.75	5.98	54.28	12.19	4.45	44.72	6.73	6.65
Optimum-1	64.16	10.15	6.32	54.30	10.82	5.02	44.72	6.55	6.81
Improvement	/	/	+5.69%	/	/	+12.81%	/	/	+2.41%
Baseline	64.28	10.75	5.98	54.28	12.19	4.45	44.72	6.73	6.65
Optimum-2	64.59	10.33	6.25	54.30	10.20	5.34	44.72	6.17	7.19
Improvement	/	/	+4.52%	/	/	+20.00%	/	/	+8.12%

Results in Table 8 show that aerodynamic performance when lift balances weight of aircraft within wide speed range has been further improved. From the optimization result it can be concluded that indicating that both planar shape and profile shape optimization can help to improve comprehensive performance over wide Mach-number-range.

5.3 Planform/profile integrated shape optimization

Aerodynamic performance of the baseline wing over wide Mach-number-range has been greatly enhanced through planar shape and profile shape optimization respectively. And in this section, planform\profile integrated shape optimization is further conducted, in which planform parameters are slightly adjusted and profile variables are further optimized. The math model of optimization is the same with that in section 5.2, and only the optimization result is discussed here. The convergence history of the objective function is plotted in Figure 23.

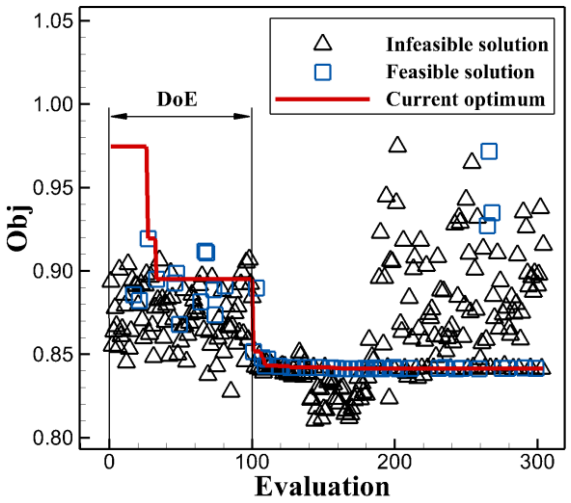

Figure 23 Convergence history and infill sampling in optimization of profile shape

Figure 24 shows a comparison of planar shapes of baseline and optimized wings, the geometric variables of plane is listed in Table 9. Figure 25 shows a comparison of geometric shapes of baseline airfoils (NPU-Hyper-04) and optimized airfoils at root, kink, and tip. It can be found that the leading edge of upper surface of the newly optimized airfoils have more obvious concave deformations, and the local curvature at trailing edge of lower surface of optimized wings has become further smaller.

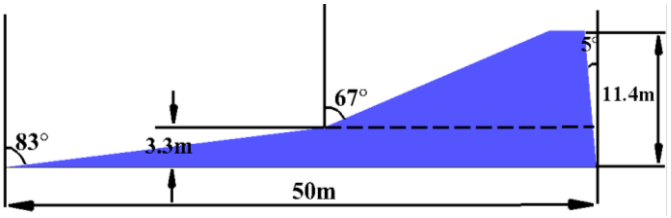

(a) Planar shape of baseline

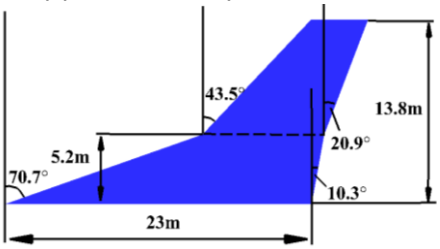

(b) Planar shape of wing obtained by planar shape optimization

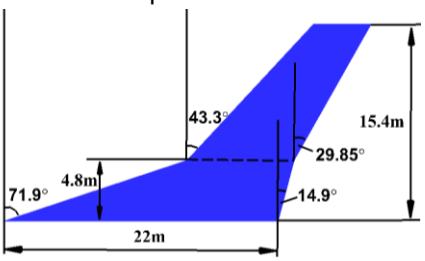

(c) Planar shape of wing obtained by plan/profile integrated optimization

Figure 24 - Comparison of planar shape between the optimized wings and baseline

Table 9 the design space of wing's planar shape

shape parameters	Baseline	Optimized wing	Optimized wing
wing area	224.56m^2	140.93m^2	140.93m^2
inner wing leading edge sweep angle	83°	70.65°	70.65°
outer wing leading edge sweep angle	67°	43.47°	43.47°
inner wing trailing edge sweep angle	5°	-10.31°	-10.31°
outer wing trailing edge sweep angle	5°	-20.93°	-20.93°
kink chord	0.4550	0.3972	0.3972
wingtip chord	0.0600	0.1856	0.1856

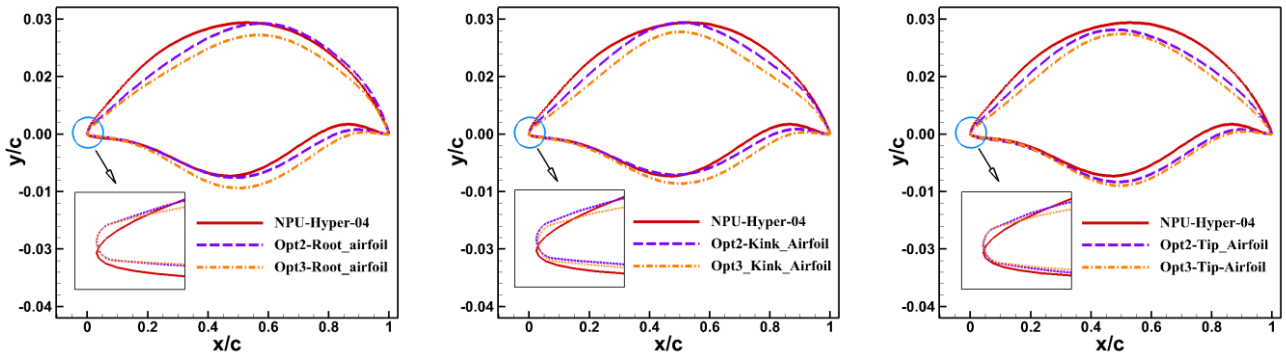

a) Root b) Kink c) Tip

Figure 25 Comparison of geometric profile at root, kink and tip of double-delta wing

Figure 26 and Figure 27 are comparison of $(C_L / C_D) - L$ curves in supersonic and hypersonic conditions. The vertical dashed lines in the two figures indicate values of corresponding weight in supersonic and hypersonic flight respectively. From intersection point of $(C_L / C_D) - L$ curves and the dashed lines, it can be seen the usable L/Ds of Opt-3 when lift balances weight have been further increased both at supersonic and hypersonic states. The detailed data of dimensional force and corresponding L/Ds in three design states is shown in Table 10. The supersonic usable L/D of Opt-3 when aerodynamic lift balances the weight is further increased to 5.32, which is 19.55% more than that of baseline wing. And the hypersonic usable L/D is further improved to 7.24, which is 2.71% than that of baseline wing.

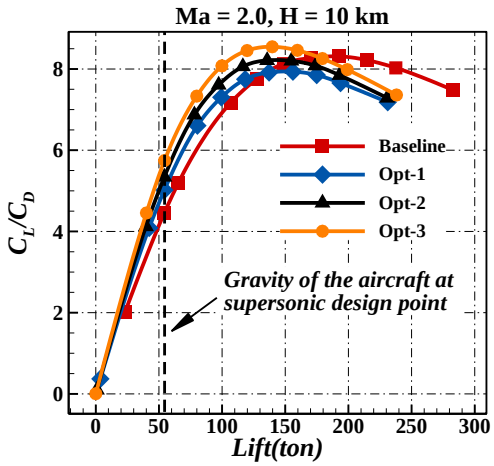

Figure 26 Comparison of $(C_L / C_D) - L$ curve at supersonic typical state $(Ma = 2.0, H = 10km)$

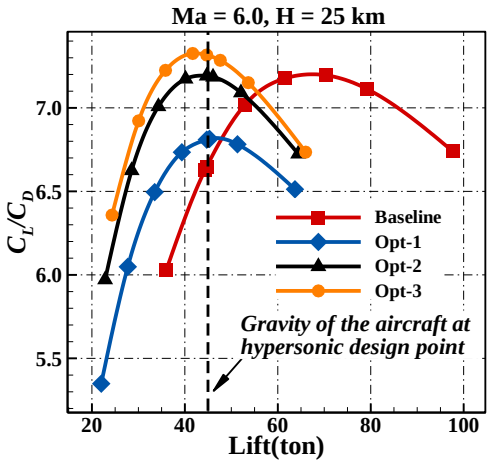

Figure 27 Comparison of $(C_L / C_D) - L$ curve at supersonic typical state $(Ma = 6.0, H = 25km)$

Table 10 Comparison of dimensional force and *L/D* between optimized wings and baseline

	Typical take-off state $(Ma = 0.3, H = 0km, \alpha = 10°)$			Supersonic design point $(Ma = 2.0, H = 10km)$			Hypersonic design point $(Ma = 6.0, H = 25km)$		
	Lift (ton)	*Drag (ton)*	*L/D*	*Lift (ton)*	*Drag (ton)*	*L/D*	*Lift (ton)*	*Drag (ton)*	*L/D*
Baseline	64.28	10.75	5.98	54.28	12.19	4.45	44.72	6.73	6.65
Opt-1	64.16	10.15	6.32	54.30	10.94	5.02	44.72	6.55	6.81
Improvement	-0.19%	/	+5.69%	/	/	+12.81%	/	/	+2.71%
Baseline	64.28	10.75	5.98	54.28	12.19	4.45	44.72	6.73	6.65
Opt-2	64.20	10.33	6.25	54.30	10.20	5.34	44.72	6.17	7.19
Improvement	-0.12%	/	+4.52%	/	/	+20.00%	/	/	+8.12%
Baseline	64.28	10.75	5.98	54.28	12.19	4.45	44.72	6.73	7.32
Opt-3	63.65	10.64	6.07	54.30	9.14	5.75	44.72	5.95	7.51
Improvement	-0.98%	/	+1.5%	/	/	+29.21%	/	/	+10.08%

6. Conclusions

In this article, optimization method based on surrogate model is used to address the challenges of aerodynamic shape optimization of a hypersonic aircraft over a wide Mach-number range. Kriging surrogate model and a parallel infill-sampling method as well as multi-round strategy are employed to address the lager-computational cost when Reynolds-averaged Navier-Stokes flow solver is adopted in the optimization. The result shows that the wing has a reasonable amount of maximum lift-to-drag ratio(L/D) but insufficient useable L/D when flying in different speed ranges, which is

especially severe at supersonic state and leads to terrible overall aerodynamic performance. And a global optimization method based on surrogate models is developed to address this problem. Then aerodynamic shape optimization based on high-fidelity CFD (computational fluid dynamics) simulations is conducted for a double-delta wing. The optimized wings are further evaluated and compared with the baseline wing at different flow regimes. The results show that hypersonic useable L/D of the optimized wing is increased by 10.08% and the supersonic useable L/D increased by 29.21%, and better performance over a wide Mach-number range is obtained.

Some conclusions can be drawn as below:

1) A wide-Mach-number wing is very difficult or impossible to fly at maximum L/D at every speed range, and the design objective should be to improve the usable L/Ds rather than maximum L/Ds, and the constraint of lift matching should be considered in design optimization of wide-Mach-number-range configuration.

2) Planform shape optimization is an important way to relieve the problem of lift matching. By adjusting wing area and other planform parameters, the phenomenon that lift is excessive in some speed range can be relieved, and the useable L/D can be closer to the maximum L/D. Planform optimization should be carried out firstly in wide-Mach-number-range aerodynamic shape optimization considering lift matching.

3) Profile shape optimization can help to reduce drag, but it has smaller effect on the lift characteristics of wing, so its capability to improve the problem of lift matching is limited.

4) Wing with medium aspect ratio and medium sweep angle has better wide-Mach-number-range aerodynamic performance. Although wing that features large sweep angle and low aspect ratio has larger maximum L/Ds at supersonic and hypersonic states, such wing needs larger area to provide take-off lift due to its terrible low-speed characteristics, which in turn makes flying states when lift matches weight at supersonic and hypersonic state severely deviates from maximum L/D states, and the usable L/Ds are unsatisfactory.

Beyond the scope of this work, wide-Mach-number-range aerodynamic design optimization considering lift matching should be further carried out on the whole aircraft, as the fuselage also provides a proportion of lift.

7. Acknowledgement

This research was supported by the National Natural Science Foundation of China grant (Nos. 11972305 and 11772261), the National Numerical Wind Tunnel Project Number 2019ZT6-A12 and 2018-ZT1A03, Shaanxi Science Fund for Distinguished Youth Scholars under grant number of 2020JC-13.

8. Contact Author Email Address

Zhong-Hua Han*, Professor, hanzh@nwpu.edu.cn, corresponding author

9. Copyright Statement

References

[1] Joyce P J, Pomroy J B, Grindle L. The Hyper-X launch vehicle: Challenges and design considerations for hypersonic flight testing. AIAA-2005-3334, 2005.

[2] Matthew P B, Steven P S. Effect of freestream noise on roughness-induced transition for the X-51A forebody. *Journal of Spacecraft and Rockets*, 2008, 45(6): 1106-1116.

[3] Sziroczak D, Smith H, A review of design issues specific to hypersonic flight vehicles. *Progress in Aerospace Sciences*, 84 (2016) 1-28.

[4] Liu F, Han Z H, Zhang Y, et al. Surrogate-Based Aerodynamic Shape Optimization of Hypersonic Flows Considering Transonic Performance. *Aerospace Science and Technology*, 2019, 93(10): 105345.

[5] Ueno A, Suzuki K. CFD-based shape optimization of hypersonic vehicles considering transonic aerodynamic performance. *Transactions of the Japan Society for Aeronautical & Space Sciences*, 2008, 52(176): 65-73.

[6] Ueno A, Taguchi H, Suzuki K. Aerodynamic shape optimization of hypersonic airliners considering multi-design-point. International congress of the aeronautical sciences, 2010.

[7] Okamura N, Honami S, Taguchi H, et al., A study on modification of low-speed aerodynamic performance of hypersonic transportation. AIAA 2012-0019, 2012.

[8] Han Z H, Xu C Z, Zhang L, et al. Efficient aerodynamic shape optimization using variable-fidelity surrogate models and multilevel computational grids. *Chinese Journal of Aeronautics*, 2020, 33(1): 31-47.

[9] Zhang K S, Han Z H, Gao Z J, et al. Constraint aggregation for large number of constraints in wing surrogate-based optimization. *Structural and Multidisciplinary Optimization*, 2019, 59: 421-438.

[10] Han Z H, Xu C Z, Qiao J L, et al. Recent progress of efficient global aerodynamic shape optimization using surrogate-based approach. *Acta Aeronautica et Astronautica Sinica*, 2020, 41(5): 25-65.

[11] Godard J L. F6 model tests in the ONERA S2MA wind tunnel. The 2nd AIAA CFD Drag Prediction Workshop. Reston: AIAA 2004-0556, 2003.

[12] Wilcox F, Birch T, Allen J. Force, surface pressure, and flow field measurements on a slender missile configuration with square cross-section at supersonic speeds. Applied Aerodynamics Conference and Exhibit, 2004.

[13] Han Z H. SurroOpt: A Generic Surrogate-based Optimization Code for Aerodynamic and Multidisciplinary Design. 30th Congress of the International Council of the Aeronautical Sciences, ICAS 2016.

[14] Han Z H. Kriging Surrogate Model and Its Application to Design Optimization: A Review of Recent Progress. *Acta Aeronautica et Astronautica Sinica*, 2016, 37(11): 3197-3225.

[15] Weingertner S. SAENGER-the reference concept of the German hypersonic technology program, AIAA-1993-5161, 1993.

[16] Kuczera H, Sacher P, Krammer P. The German hypersonic programme-status report: AIAA 1991-5001, 1991.

[17] Sun X C, Han Z H, Liu F, et al. Design and analysis of hypersonic vehicle airfoil/wing at wide-range Mach numbers. *Acta Aeronautica et Astronautica Sinica*, 2018, 39(6): 121737.